

Regional Resolving Power of Combined MEG/EEG

Pflieger, ME, Greenblatt, RE, and Kirkish, J
Source Signal Imaging, Inc., San Diego, USA

Corresponding Author: Mark E. Pflieger, Address: Source Signal Imaging, Inc.,
2323 Broadway, Suite 102, San Diego, CA 92102 USA,
Fax: +1-619-234-9934, Phone: +1-619-234-9935, Email: mep@sourcesignal.com.

ABSTRACT

Different modeling frameworks (such as error analyses for dipole localization [Fuchs, 1998; Huizenga, 2001]; crosstalk and point spread analyses for linear estimators [Liu, 2002]; etc.) have demonstrated improved three-dimensional (3D) resolution for combined MEG/EEG (or EMEG) source estimation. Complementary to these, an empirical analysis of 2D surface data suggested that MEG and EEG information content could be superadditive [Pflieger, 2000]. Taking a hybrid approach in the present study, we made simulations within a regional activity estimation (REGAE, [Pflieger, 2001]) framework, which quantifies the ability of EMEG to discriminate brain activity originating within a 3D region of interest (ROI) from simultaneous non-ROI activity. Two metrics were employed: Kullback-Leibler divergence (KLD) and area under the receiver operator characteristic curve (AUROC). High-density sensor configurations (248 magnetometers, 256 electrodes) were combined with a gray matter source space model (7931 dipole triples, maximum entropy activities), assuming magnetic 3-shell sphere and electric BEM head models. Superadditive KLD was observed frequently across 89 representative brain ROIs and 3 ROI sizes (5, 10, and 15 mm radii), especially for regions already fairly visible to each modality. We also report an observed functional relationship between AUROC and KLD.

KEY WORDS

Magnetoencephalography, Electroencephalography, Brain electrical activity mapping, Information theory, Regional activity estimation.

THEORY

Macroscopic ionic currents in the brain generate measurable extracranial fields that may be detected by MEG and EEG sensors. Regional activity estimation (REGAE) is a framework for discriminating (in extracranial measurement space) source signals that originated inside a brain region of interest (ROI) from all other source signals, i.e., those that simultaneously may have been generated outside the ROI [Pflieger, 2001]. The discrimination is made via a measurement space *norm* that ideally should be indifferent to contributions from non-ROI generators while it assigns smaller or larger values to measurement vectors that had (respectively) smaller or larger contributions from ROI source signals. An ℓ^2 -norm on the measurement space may be characterized by a square matrix \mathbf{H} (m -by- m , m = number of channels) such that vector \mathbf{x} has norm $|\mathbf{x}|_{\mathbf{H}} \equiv \sqrt{\mathbf{x}^t \mathbf{H} \mathbf{x}}$. In turn, \mathbf{H} may be decomposed as $\mathbf{H} = \mathbf{E}^t \mathbf{E}$, where \mathbf{E} is an *estimator matrix*, and $\mathbf{y} = \mathbf{E} \mathbf{x}$ is a dimensionless vector, the magnitude of which reflects an estimate of total ROI “activity” (noting that the Euclidean norm of \mathbf{y} is the \mathbf{H} -norm of \mathbf{x}). Typically in practice, the ROI-specific estimator matrix \mathbf{E} may be reduced to a d -by- m matrix, where the *estimator dimension* d is considerably smaller than m . That is, only d directions in measurement space are relevant for discriminating ROI signals from non-ROI signals.

For defining both ROI and non-ROI, the REGAE framework utilizes a *geometric source space model*. Possible locations and directions of current are represented (typically) by thousands of unit dipole elements in brain gray matter (with or without a cortical orientation constraint). An ROI is defined as a “mask” that maps brain locations to values ranging between 1 (inside ROI) and 0 (outside ROI). For example, an ROI may be defined within gray matter via a central location (where the mask value is 1) and a function that tapers with distance (e.g., Gaussian; using either a 2D surface metric or a 3D metric modified by exclude regions). Thus, an ROI mask may be represented as an n -dimensional vector \mathbf{r} (n = number of dipole elements). The *sensor geometry* and a *volume conductor model* are required to calculate a gain matrix \mathbf{G} (m -by- n) from dipole elements to sensors (or to channels derived from linear combinations of sensors). A *source statistics model* is posited, which consists of a “prior” distribution of source currents over the source space geometry. For example, an unconstrained maximum entropy distribution posits identical and independent activities over all source locations (alternatively, constraints may be introduced). Assuming a mean zero Gaussian distribution, the source statistics model may be characterized by a source signal covariance matrix \mathbf{S} (n -by- n). Then the measurement space statistics, also Gaussian, have covariance

$$\mathbf{C} = \mathbf{G}\mathbf{S}\mathbf{G}^t. \quad (1)$$

Note that \mathbf{C} (m -by- m) has contributions from both ROI and non-ROI portions of the source space. Without ROI activity, the covariance would be

$$\mathbf{C}_{1-r} = \mathbf{G}(\mathbf{I} - \text{diag}(\mathbf{r}))\mathbf{S}(\mathbf{I} - \text{diag}(\mathbf{r}))\mathbf{G}^t. \quad (2)$$

Because (1) and (2) have the non-ROI activity in common, the sole differentiating feature is presence versus absence of ROI activity. The norm we seek should utilize all information available for discriminating these two distributions. This information may be quantified as the Kullback-Leibler divergence (KL-divergence, KLD) which, for two mean zero Gaussian distributions, is one half of the trace of the following matrix [Kullback, 1959]:

$$\mathbf{H}_r \equiv (\mathbf{C} - \mathbf{C}_{1-r})(\mathbf{C}_{1-r}^{-1} - \mathbf{C}^{-1}). \quad (3)$$

As a REGAE norm matrix, this has several desirable properties: (i) all available information for detecting ROI activity in the presence of non-ROI activity is utilized, (ii) the norm of a measurement vector increases with increasing ROI activity (and is zero when there is no ROI activity), and (iii) it is indifferent to non-ROI activity. However, to the extent that ROI and non-ROI projections overlap in measurement space, REGAE inevitably will miss some ROI activity that produces non-zero measurements (i.e., those which are uninformative for discriminating ROI activity from non-ROI activity). Note that the inverses of (3) ordinarily exist: Due to the projection of many source space elements to considerably fewer sensors, both covariance matrices are expected to be nonsingular. Thus, REGAE estimation does not require the Moore-Penrose generalized inverse.

METHODS

Using EMSE Suite software tools, we constructed a geometric source space model from an individual subject’s T1-weighted MRI. A segmented gray matter region (both cortical and non-cortical) was populated with 23,793 dipole elements at 7931 locations (3 orthogonal dipoles per location), tightly packed with a 5 mm minimum distance constraint. A random subset of locations was auto-selected based on a 25 mm minimum distance constraint, which produced 89 ROI centers that loosely covered the entire source space (see Figure 3, row 1). At each ROI center, ROIs of three different sizes were obtained by intersecting the source space with 3D spherical Gaussian distributions having standard deviations of 5, 10, and 15 mm. As shown in Figure 1, MEG sensor geometry was based on a 248-channel commercial system (4-D Neuroimaging); likewise, EEG sensor geometry was based on a 256-channel commercial system (Neuroscan). Both configurations were registered to the subject’s whole-head MRI. A magnetic gain matrix (248-by-23,793) was computed using a 3-shell sphere head model, and an average-referenced electric gain matrix (256-by-23,793) was computed using a 3-compartment boundary element model

(using scalp, outer skull, and inner skull meshes obtained from the subject’s MRI). We used an identity source signal covariance matrix. For each ROI, the REGAE estimator and its associated KL-divergence were computed for EEG only, MEG only, and combined EMEG cases. MEG and EEG measurements were converted to a common system by normalizing with respect to non-ROI variances and pre-whitening with respect to non-ROI covariances [Pflieger, 2000]. Area under the receiver operator characteristic curve (AUROC) was calculated by simulating 200 instances of both ROI+non-ROI data and non-ROI-only data [Pflieger, 2001]. Additivity ratios for KL-divergence were calculated as $KLD(EMEG)/(KLD(MEG)+KLD(EEG))$.

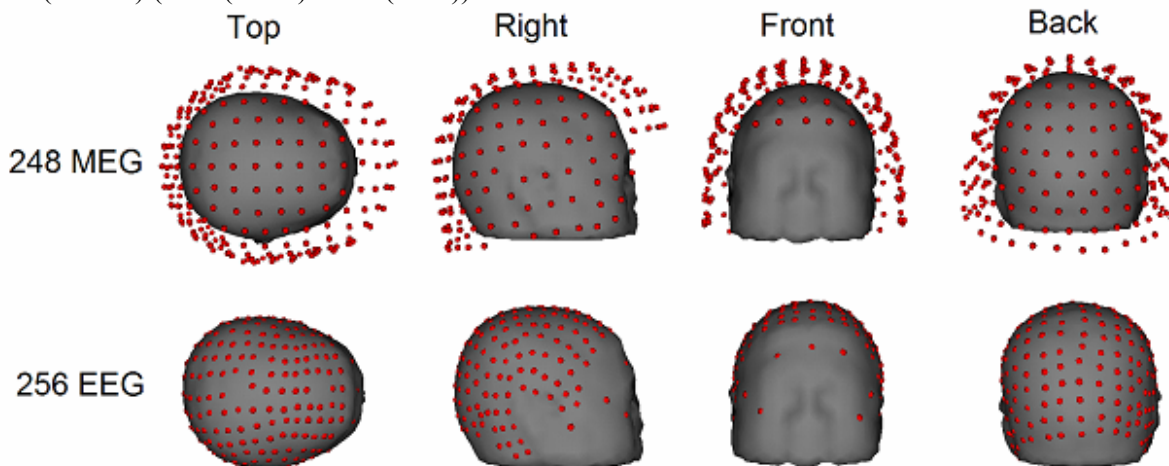


Figure 1. Sensor configurations for MEG (top row) and EEG (bottom row).

RESULTS

AUROC. Figure 2 shows AUROC averages, minima, and maxima obtained across all 89 ROIs for each modality (EEG, MEG, EMEG) and ROI radius (5, 10 & 15 mm). EEG and MEG compare closely on average, and the average bimodal improvement is considerable across all radii. Bimodal improvement is essentially nil for worst case ROIs (those with minimum AUROC), but may considerably outperform average improvement for best case ROIs.

KL-divergence. Similarly, Table 1 shows KL-divergence averages and maxima. All minima were near zero (not shown). All standard deviations and averages have comparable magnitudes. EEG best cases exceed MEG best cases. On the other hand, MEG is more consistent across ROIs, as manifested by lower standard deviations. Figure 3 plots KLD results for representative ROIs having 10 mm radii.

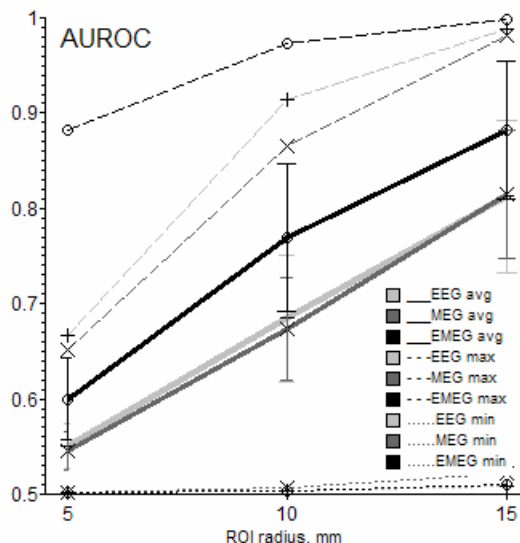


Figure 2. AUROC averages and ranges.

	5 mm		10 mm		15 mm	
	avg±sd	max	avg±sd	max	avg±sd	max
EEG	0.09±0.11	0.55	1.13±1.43	6.00	6.30±6.09	24.7
MEG	0.06±0.09	0.46	0.89±0.93	4.36	4.34±3.80	16.4
EMEG	0.20±0.27	1.59	2.85±2.79	11.6	13.1±11.1	46.3

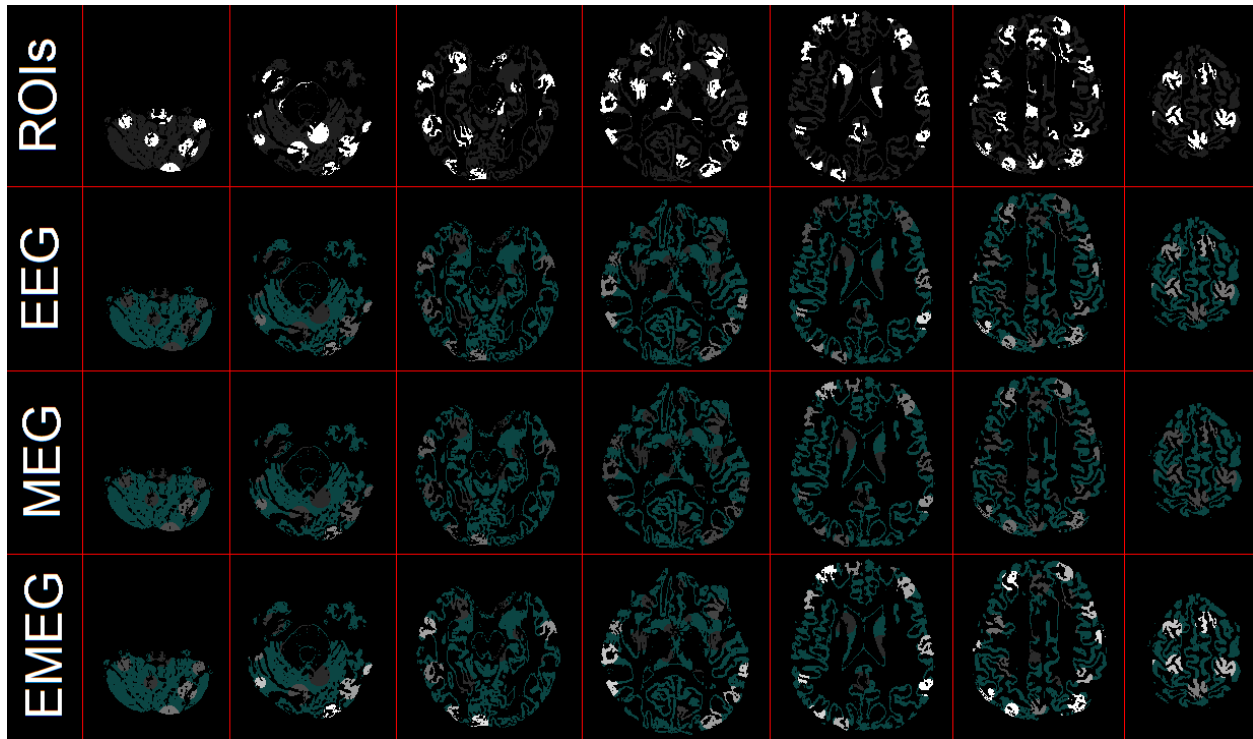


Figure 3. 10 mm radius ROIs and associated KLD results for EEG only, MEG only, and combined EMEG. Columns correspond to seven axial slices of segmented gray matter, separated by about 20 mm, from inferior (cerebellum, first column) to superior (near top of the brain, last column). In row 1, gray matter ROIs within 10 mm of 89 randomly selected points are depicted via highest intensity pixels. KLD results are mapped to the same ROIs in rows 2-4, with highest intensity pixels (as in row 1) corresponding to KLD=10, and with lowest gray intensity pixels (as in row 1) corresponding to KLD=0.

Relationship between AUROC and KL-divergence (KLD). Figure 4 plots results for all ROIs, modalities, and ROI radii, which demonstrates that a consistent log-log linear relationship emerged between a function of AUROC, $g(\text{AUROC}) = -\log(2-2\text{AUROC})$, and KL-divergence. Linearity breaks down at the lower left end of the plot, probably due to approaching limits of numerical resolution for the smallest KL-divergence and AUROC values. Because log-log linearity implies a power law, the functional relationship obtained after symbol manipulation is

$$\text{AUROC} = 1 - 0.5 \exp\{-e^B (\text{KLD})^A\} \quad (4)$$

with $A = \text{slope}$ and $B = \text{y-intercept}$; our results put these at approximately 0.5 and -0.5 , respectively.

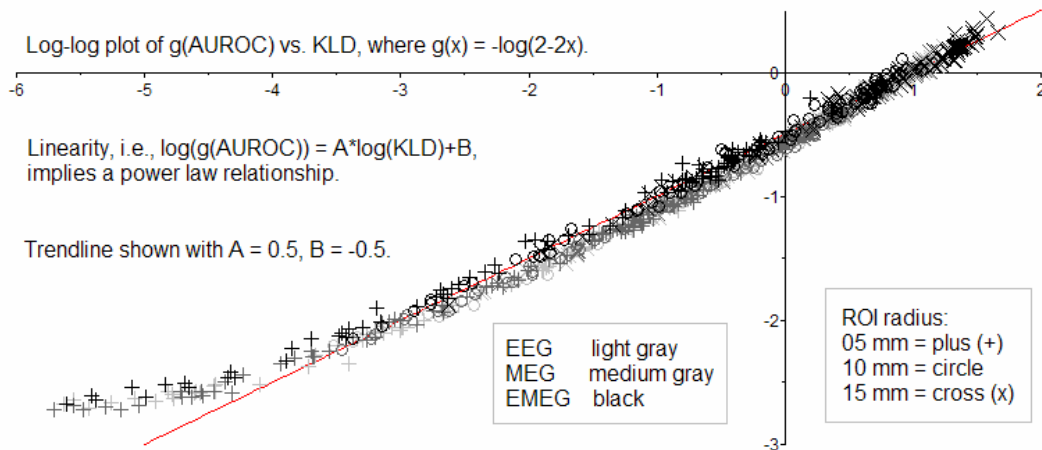


Figure 4. Functional relationship of AUROC to KL-divergence (plot for all conditions).

Additivity ratios. “Superadditivity” implies that the KLD information content of the bimodal EMEG data exceeds the sum of unimodal KLDs (for EEG alone and for MEG alone), i.e., that the additivity ratio exceeds 1.0. Inspection of Table 1 reveals that the averages and maxima were superadditive for all ROI sizes (e.g., the additivity ratio for the KLD averages for the 10 mm radius case is 1.41). In addition, we inspected additivity ratios for each ROI and found that 93% were superadditive. Of these, 76% had a pattern of decreasing additivity ratio with increasing ROI radius. The average of 10 mm radius additivity ratios across the 89 ROIs was 1.29.

DISCUSSION

This simulation study demonstrates that, in principle, combined electromagnetic source estimation may be highly beneficial within the REGAE framework: An ROI with fair “visibility” for each modality may become significantly more visible when both modalities are utilized simultaneously. However, ROIs with very poor visibilities in both modalities are unlikely to benefit from bimodal estimation. Visibility in the REGAE context means the ability to distinguish statistically brain activity of ROI origin from that originating anywhere else in the source space. As visualized in Figure 3, ROIs with poorer visibility have deeper locations, whereas superficial ROIs generally have excellent visibility with both modalities. Additionally, we have observed ROIs with asymmetric visibility (MEG substantially greater than EEG, or vice versa) with highly superadditive bimodal results (e.g., for deep inferior occipital ROI 27, 10 mm case, $KLD(EEG) = 0.364$, $KLD(MEG) = 4.36$, and $KLD(EMEG) = 8.14$; the additivity ratio is 1.72). Thus, modest visibility in one modality may substantially boost good visibility in the other modality.

As discussed in [Pflieger, 2000], superadditivity of information content is possible only when both modalities cooperate to enhance the *contrast* between signal (ROI activity) and noise (non-ROI activity). In particular, the essential contrast operation is spatial pre-whitening of the measurements with respect to the non-ROI covariance statistics, which places MEG and EEG measurements into a common dimensionless system. Information derived from *cross*-covariances between EEG and MEG channels enables the possibility of superadditivity. On the other hand, if each channel is normalized only by its own standard deviation, without using the full bimodal sensor covariance matrix (that is, if the off-diagonal entries are assumed to be zero), then the goal of placing MEG and EEG measurements in a common system is met, but the possibility of superadditivity is sacrificed.

Although our results show substantial equality between EEG and MEG, this study is limited by the assumption of perfect head models. This introduces a bias in favor of EEG, because MEG is more robust in the presence of head modeling errors. Previously, in an EEG simulation study, we showed that head modeling errors can reverse gains that otherwise would be expected for higher sensor densities [Pflieger, 2002], presumably because these errors (expressed as percentages) increase with higher spatial frequencies. To overcome this limitation, we are studying a REGAE estimator designed for a *distribution* of head models, where the distribution stems from uncertain geometries and conductivities. Thus, we plan to address the bias issue in this context by simulating a plausible distribution of head modeling errors.

We also plan to address another limitation in a follow-up study, namely, that the source space model did not employ orientation constraints, i.e., that all orientations were assumed to contribute equally for each location in the source space. This introduces a bias in favor of MEG, because MEG sensitivity varies with orientation, whereas EEG in principle does not.

To our knowledge, this is the first report of an observed functional relationship between AUROC and KLD, as expressed in equation (4). This empirical relationship holds up well over all conditions of this study, i.e., all brain locations, region sizes, and measurement modalities.

ACKNOWLEDGEMENTS

This work is supported by NIMH grant R44 MH64343. Don Rojas kindly provided a dataset utilized to construct simulations.

REFERENCES

Fuchs M, Wagner M, Wischmann H-A, Köhler T, Theissen A, Drenckhan R, Buchner H. Improving source reconstructions by combining bioelectric and biomagnetic data. *Electroencephalogr Clin Neurophysiol* 1998;107(2):93-111.

Huizenga HM, van Zuijlen TL, Heslenfeld DJ, Molenaar PCM. Simultaneous MEG and EEG source analysis. *Phys Med Biol* 2001;46:1737-51.

Kullback S. *Information Theory and Statistics*. Mineola, New York: Dover Publications; 1959 (republished 1997).

Liu AK, Dale AM, Belliveau JW. Monte Carlo simulation studies of EEG and MEG localization accuracy. *Hum Brain Mapp* 2002;16:47-62.

Pflieger ME, Simpson GV, Ahlfors SP, Ilmoniemi RJ. Superadditive information from simultaneous MEG/EEG data. In: C.J. Aine et al. (eds.), *Biomag 96*, Vol. II; 21154-7;2000.

Pflieger ME, Greenblatt RE. A regional approach to M/EEG source estimation: characterizing the tradeoff between spatial resolution and signal discriminability [abstract]. *NeuroImage* 2001;13:S219.

Pflieger ME, Greenblatt RE. Interaction of head model misspecification with EEG electrode density in the detection of regional brain signals [abstract]. *NeuroImage* 2002;16(2):CD-ROM.